

Multi-Layered Membrane Structures with Curved Creases for Smooth Packaging and Deployment

Nicolas Lee* and Sergio Pellegrino[†]

California Institute of Technology, Pasadena, CA 91125

We present a design for a deployable multi-layered membrane structure that uses a curved crease pattern to enable smooth wrapping around a spool. The crease pattern is parameterized to enable a variety of designs, and a specific implementation was selected based on an existing patch antenna array design. We constructed a prototype structure based on this geometry, and conducted deployment tests to measure the deployment force profile required to unfold the structure and to unwrap it from a spool. We find that the deployment force for unwrapping is significantly higher than for unfolding. These force profiles are repeatable over multiple deployments and the global trends do not depend on deployment rates over the range tested, between 1 and 8 mm/s. However, the local dynamic behavior can depend on deployment rate.

I. Introduction

In this paper, we present a design for a multi-layered membrane structure that can be deployed from a cylindrical spool. This type of deployable membrane structure has potential applications in spacecraft systems. Deployable systems in general are a crucial aspect of spacecraft design because of their ability to address and satisfy constraints imposed during different mission phases. During launch, the rocket fairing and the acoustic environment impose geometric and stiffness constraints that are often incompatible with the performance requirements for large area systems during the operational phase. Maximizing the area of a spacecraft component is essential for many systems where performance is directly related to a captured flux quantity. Obvious examples include solar arrays and communications antennas, but deployed area is also a factor for systems including but not limited to telescopes, radar, and in situ dust detectors and collectors. While many spacecraft use deployable technology, it remains a significant risk with a history of many failures and anomalies. These include jammed solar panel hinges (e.g. Intelsat 19¹) and dish antennas (e.g. Galileo's high gain antenna² and SkyTerra 1's 22-meter L-band antenna³), incomplete tether deployments (e.g. MAST⁴), and broken tethers and booms (e.g. ARTEMIS, TSS-1R⁵). Membrane systems in particular are prone to unexpected behavior during deployment, including for example the tearing of the Znamya 2.5 solar reflector,⁶ and premature expansion of components of the Inflatable Antenna Experiment.⁷ The dependence of future spacecraft on deployable systems necessitates a better understanding of their behavior through all mission phases in order to characterize and reduce overall mission risk.

Deployable spacecraft systems can range from extremely lightweight, such as solar sails that use membranes only several microns thick, to relatively thick rigid panels such as the solar arrays deployed on communications satellites. For some applications, the rigidity of a panel is not required and the complexity of hinges undesirable. In some cases, like proposed large radar arrays for Earth observation, discrete panels are too heavy to be feasible but the thin membranes used in solar sails are too thin to support the electronic components associated with each antenna.

In this paper, we present a design for a deployable thick-membrane structure for applications that require an intermediate solution between thin membranes and rigid panels, using a membrane that is thick enough to support electronics but is thin enough to be flexible. In particular, we focus on the implementation of a planar structure that is compatible with an existing design for a membrane patch antenna array for synthetic aperture radar (SAR), as illustrated in Figure 1. This structure is composed of two parallel membrane surfaces joined to each other by a set of ribs that determine the thickness of the structure. The membranes are creased using a curved design to enable tight packaging around a hub such that the structure can be packaged for launch into a volume with dimensions smaller

*W. M. Keck Institute for Space Studies Postdoctoral Scholar, Graduate Aerospace Laboratories, 1200 E. California Blvd. MC 301-46. nnlee@caltech.edu

[†]Joyce and Kent Kresa Professor of Aeronautics and Professor of Civil Engineering, Graduate Aerospace Laboratories, 1200 E. California Blvd. MC 301-46. AIAA Fellow. sergiop@caltech.edu

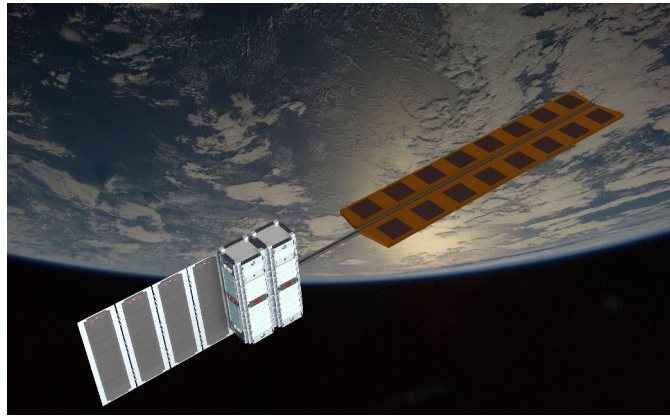


Figure 1. Rendering of a 6U CubeSat concept with membrane antenna array. In this image, the membrane antenna is shown with 16 patch antenna elements and is supported by a longitudinal boom. The membrane would theoretically deploy out of a 3U volume, with the spacecraft bus occupying the other 3U. Background image courtesy NASA.

than the length of an uncreased panel. The full structure is 29.2 cm in width and 124.8 cm in length, with a 1.27 cm separation between the two layers. A full-size prototype structure was constructed (Figure 2) and used to conduct deployment experiments.

Through these experiments, we found that the dominant force resisting deployment as the structure is unfolding results primarily from the unwrapping of the membrane from a hub, but that this deployment force can be exceeded by the tension required at the end of deployment to ensure that the structure is adequately flat. The measured force profiles were repeatable over multiple deployments and the global trends did not appear to depend on deployment rates over the range tested, between 1 and 8 mm/s. We also found that the deployment rate can affect the dynamic behavior of the membrane, even at relatively low rates.

Section II provides an overview of relevant background to the work described in this paper. Section III describes mathematically the crease pattern used to enable smooth wrapping of the folded structure on a cylindrical hub, including a general derivation for a parameterized structure with arbitrary dimensions and a specific design for the antenna array configuration. Section IV presents the techniques used to assemble a prototype membrane structure consistent with the geometry of the design from Section III. Deployment experiments that characterize the force profile using the prototype in a materials testing machine are described in Section V, with results presented and discussed in Section VI. Finally, Section VII provides a summary of the key findings and directions for further work in this area.

II. Background

This section highlights previous work on membrane packaging and deployment, as well as on the existing membrane antenna array configuration that our membrane structure is designed to support.

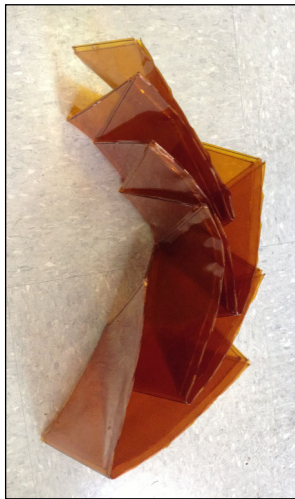
A. Membrane Packaging and Deployment

Previous work on membrane packaging and deployment spans the range between theoretical models and empirical observations. In particular, much work has been done on the problem of wrapping a membrane around a hub. Guest and Pellegrino⁸ provided an algorithm for a crease pattern to wrap a membrane around a polygonal hub by determining the 3D geometry of the crease vertices. Furuya et al.⁹ described experiments in centrifugal deployment of a wrapped membrane from a spinning hub. Recently, Zirbel et al.¹⁰ performed experiments demonstrating the deployment of a membrane with embedded rigid panels from a polygonal hub.

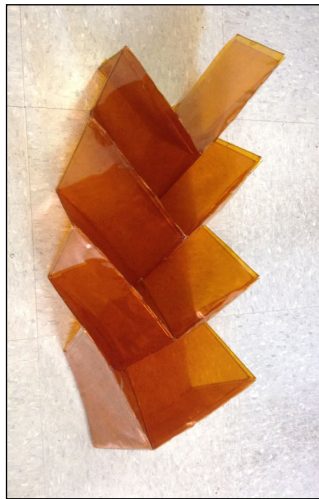
In order to enable wrapping around a round hub, Lee and Close¹¹ presented an algorithm to compute a crease pattern composed of equally spaced curved creases. In that work, creases are restricted to lie on a horizontal plane as they are wrapped around the hub. This paper extends the technique to account for the more general case where creases may not lie only on a horizontal plane. The crease pattern is applied to a membrane geometry such that multiple membrane layers can be attached to each other at a specified distance to form a thicker global structure once deployed. This membrane structure design is targeted to support a planar patch antenna array described in the following section.



(a)



(b)



(c)



(d)



(e)

Figure 2. Prototype membrane structure in several stages of deployment. (a) The packaged structure can be coiled into a package with diameter less than 10 cm. (b)-(e) As the membrane unfolds, it flattens into a structure 29.2 cm in width and 124.8 cm in length with the two membranes separated by 1.27 cm.

B. Membrane-based Patch Antenna Array

A phased array patch antenna system has been developed at the Jet Propulsion Laboratory for L-band (1.26 GHz) SAR applications.¹³ These antenna systems are envisaged for Earth-observation missions at medium or geostationary Earth orbit (MEO or GEO), where larger arrays are required than at low Earth orbit (LEO). The higher altitude allows for revisit times on the order of minutes suitable for disaster response or future study of earthquake physics.¹²

Active arrays of up to 256 elements (in a 16×16 rectangular array) have been tested using phase-shifting transmit/receive (T/R) modules to electronically steer the main beam up to 30° .¹³ This antenna array is composed of two membrane layers, with the radio frequency feed network, T/R electronics and ground plane on one membrane, and radiating patches on the other. Slots in the ground plane allow the feed network to couple with the radiating patches so that no *physical* electrical connection is required between the layers. The patch elements are 8.89 cm (3.5") square, positioned in a rectangular array with a spacing of 15.24 cm (6"). Previous passive antenna designs have also used a three-layer configuration so that the feed network is placed a greater distance away from the ground plane.¹⁴

These prototypes were designed with $50 \mu\text{m}$ DuPont™ Kapton® polyimide film^a as the membrane substrate. Thinner membranes would require a corresponding decrease in the width of the feed network to maintain impedance, and is limited by fabrication constraints. The most recent prototypes have used conventional flexible printed circuit board (PCB) fabrication techniques by etching a copper foil layer. Potential avenues for overcoming this constraint could involve alternative circuit fabrication techniques, such as materials printing with conductive inks.

We used the existing two-layer antenna array design to motivate the development of the multi-layered membrane structure described in this paper. This deployable structure, using the crease pattern described in the next section, provides one possible approach toward implementing the antenna array as a spacecraft payload.

III. Membrane Crease Design

In order to allow the membrane structure with multiple layers to collapse and lie flat, we chose to use the same crease pattern on all layers. The crease pattern for each membrane is based on the beech leaf fold described by Kobayashi et al.¹⁵ and shown in Figure 3. In this section, we describe the general parameters governing the folding behavior of this crease pattern, as well as the modifications necessary to allow the folded membrane to wrap smoothly around a spool while accounting for the membrane thickness τ . We then describe the specific crease pattern selected to be compatible with the antenna array design. Finally, we discuss alternative possibilities for arranging multiple membrane layers in the structure.

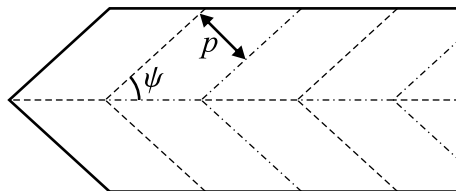


Figure 3. Kobayashi's beech leaf folding pattern with relevant parameters illustrated. Valley folds are denoted with dashed lines and mountain folds with dash-dotted lines. Parameters that can be varied include the crease spacing p and the crease angle ψ .

A. General Crease Pattern

The beech leaf folding pattern has two sets of diagonal creases. Each crease intersects with one from the opposite set at a centerline crease, which alternates between mountain and valley folds. The fold pattern is determined only by the spacing between the diagonal creases and by the angle they make with the centerline crease. This angle ψ between the centerline crease and the diagonal creases is constrained between 0° and 90° , with 0° corresponding to the degenerate case where the diagonal creases are parallel to the centerline and folding does not occur, and 90° corresponding to the case of maximum longitudinal compression along the centerline. To attach membrane layers to each other, vertical ribs can be attached along the diagonal creases. However, this requires that the crease angles remain constant so that the creases are parallel. The crease separation distance p is also usually constant and can be selected to provide a height $p \sin \psi$ of the folded membrane configuration.

^aDuPont™ and Kapton® are trademarks or registered trademarks of E.I. du Pont de Nemours and Company

By keeping the parameters constant over all creases, the folded configuration will have a uniform height, which simplifies the packaging process. Additionally, for some applications such as solar panels, components of a constant size must be embedded on the membrane between creases, and is more straightforward to implement on a membrane with creases at a constant spacing. However, by allowing the crease angles and separation distances to vary, it is possible to achieve favorable deployment dynamics. The kinetic energy associated with deployment varies as the deployment angle θ goes from 0° to 90° , and is greatest near the end of deployment when $\theta \approx 90^\circ$.¹⁶ With a folding pattern that has smaller crease angles at the root of the membrane and larger angles at the tip, the deployment energy profile can be tuned for greater uniformity.

The straight line crease patterns can then be adapted using curved creases to coil smoothly so that they can be packaged on a spool. The technique to determine the crease curvature has been developed previously by Lee and Close¹¹ and is based on the principle of computing the crease length in the coiled configuration to determine its required curvature in the unfolded configuration. A similar finding was determined through empirical folding experiments by Satou and Furuya.¹⁷ However, the algorithm needs to be adapted to the properties of this particular crease pattern. Specifically, the reference center line for the beech leaf crease pattern does not remain horizontally in the same plane; it zig-zags across the height of the pleat as depicted in Figure 4. This produces a longitudinal compression in the folded membrane, and results in a crease that must lie along a helical spiral in the coiled configuration.

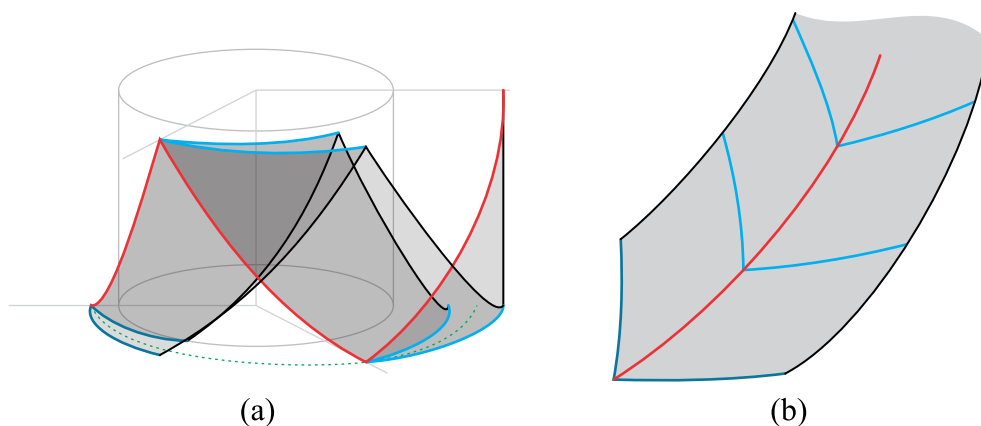


Figure 4. Sketch of the curved crease geometry in its (a) wrapped and (b) flattened configurations. The center line crease (in red) traverses along helical spiral segments as the membrane wraps around a hub. The diagonal creases (in blue) remain in a horizontal plane, but alternate creases lie on different planes.

For a structure geometry where the length is greater than the width, we can assume that the thickness of the folded membrane configuration is roughly constant and can approximate the coiled radius of the centerline as an Archimedes' spiral of the form

$$r(\theta) = r(0) + \frac{r(2\pi) - r(0)}{2\pi}\theta = r(0) + b\theta, \quad (1)$$

where θ is the angular coordinate around the hub, b is the spiral rate parameter, and $r(0)$ is the initial radius. For a total folded thickness $2h$, we have the rate parameter $b = h/\pi$. However, unlike the previous work, the path length of the crease must be projected in 3D such that

$$\begin{aligned} \xi(\theta) \cos\psi = & \frac{(b\theta + r(0))\sqrt{b^2 + (b\theta + r(0))^2}}{2b} \\ & + \frac{1}{2}b \ln \frac{\sqrt{b^2 + (b\theta + r(0))^2} + b\theta + r(0)}{\sqrt{b^2 + r(0)^2} + r(0)} \\ & - \frac{r(0)\sqrt{b^2 + r(0)^2}}{2b}, \end{aligned} \quad (2)$$

where the right-hand side is the closed form path length of the Archimedes' spiral. The curvature of the spiral is

$$\kappa = \frac{(2 + (\theta + r(0)/b)^2)}{b(1 + (\theta + r(0)/b)^2)^{3/2}}, \quad (3)$$

which can be related to the crease radius of curvature R using the relation

$$R = \left(\frac{p}{\tau}\right) \frac{1}{\kappa}. \quad (4)$$

The diagonal creases in the folding pattern do remain in a horizontal plane when the membrane is folded, and their curvature is therefore described as above but without the $\cos\psi$ projection.

Figure 5 contains a folding pattern developed using this algorithm. A similar pattern was used to fold the paper model in Figure 6, which demonstrates the ability of the folded membrane to wrap tightly and smoothly. To assess the effectiveness of this folding strategy, the packing efficiency is estimated as the volume of membrane material divided by the smallest volume of an encompassing rectangular prism. A paper membrane with an area of 400 cm^2 and thickness of 0.11 mm has a volume of 4.4 cm^3 , and was packaged into a roll with a diameter of 2.3 cm and a height of 1.5 cm , which can be contained within a rectangular volume of 7.94 cm^3 . This is a packing efficiency of 55% , which includes volumes within the spool and in the corners of the box that remain usable.

B. Crease Pattern for Membrane Antenna Array

With the membrane antenna array described in Section II.B, a practical consideration is that the creases may degrade the performance of the antenna by affecting the geometry or even the conductivity of the radiating elements. Additionally, the existing design uses T/R modules that could not be creased with the membrane. We therefore designed a crease pattern choosing parameters that would avoid creases overlapping with either the T/R modules or the patches. The goal for this design was to fit a 2×8 array onto a membrane that could package inside a 3U CubeSat volume ($10 \times 10 \times 34.5 \text{ cm}$). With the 15.24 cm antenna spacing in two dimensions, a rigid-foldable pattern based around the patches, where individual panels do not bend, would not fit within the prescribed volume. However, the

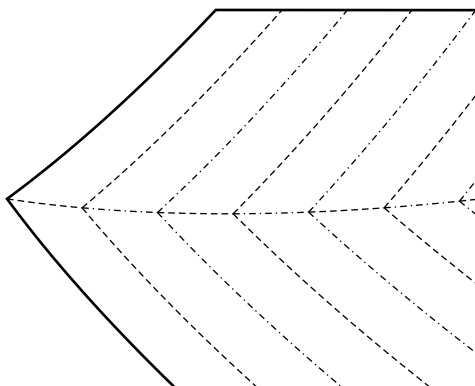


Figure 5. Beech leaf folding pattern with curved creases to enable wrapping in the folded configuration. Valley folds are denoted with dashed lines and mountain folds with dash-dotted lines. In this crease pattern, the crease angle ψ has been chosen to be 45° .

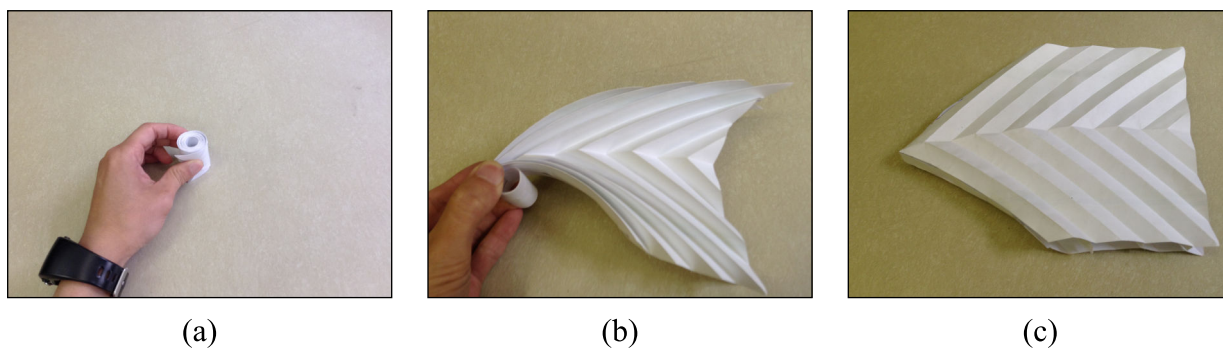


Figure 6. Paper prototype of a two-layer structure using a curved beech leaf crease pattern. These three photos show (a) the initial wrapped membrane, (b) an intermediate stage during deployment, and (c) the final deployed structure.

use of the curved crease pattern permits one linear dimension to wrap around a spool, while the other can occupy the longest dimension of the CubeSat volume.

For this crease design, the free parameters available in the design space include the crease angle ψ , the spiral parameter b , and the spool radius r_0 . In order to fit the diagonal creases between the patches, the angle ψ must be greater than 54° . However, having a large crease angle will result in a thicker folded membrane package, which would be more difficult to coil. A crease angle of 75° was selected as a compromise between these two competing objectives. The spiral parameter was computed by estimating a total folded membrane thickness of 4 mm, accounting for the additional thickness necessary to embed electronics on the surface. This yields a spiral rate of 4 mm per revolution, or 0.64 mm per radian. Because of the limited space between the two rows of patches, we desired a centerline crease with as little curvature as possible. This was accomplished by selecting the largest possible spool radius that would result in a wrapped membrane still satisfying the 10×10 cm CubeSat constraint. These geometric constraints are depicted in Figure 7. A spool radius of 4 cm was found to be adequate to satisfy the design requirements. Using these parameters, the curved crease pattern was produced, and overlaid on the rectangular patch antenna array, as shown in Figure 8.

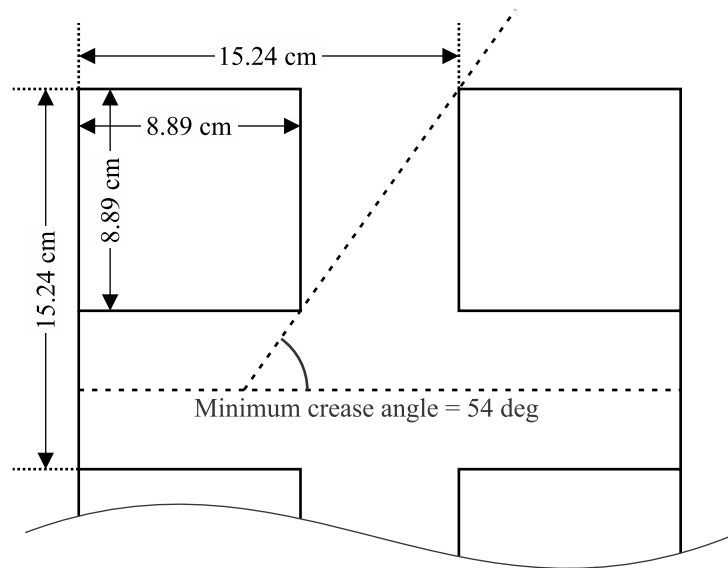


Figure 7. Antenna array dimensions and constraints on crease geometry. Each radiating patch is a square with a side length of 8.89 cm. The patches are spaced in a rectangular array at intervals of 15.24 cm in both directions. In order to avoid creasing the patch, the minimum crease angle possible using a straight-line beech leaf crease pattern is approximately 54° . When implementing a curved crease pattern, the centerline must lie within the 6.35 cm gap between patches.

C. Arrangement of Multiple Membrane Layers

Using the beech leaf folding pattern with a constant crease angle, the diagonal creases remain parallel and horizontal as the membrane folds. The corresponding diagonal creases on parallel membranes with the same crease pattern would therefore remain the same distance apart. In order to construct a multi-layered structure, these diagonal creases can be joined by a vertical rib. As the membrane structure folds, each of the rectangular cells formed by two horizontal membrane panels and the two ribs connecting them would be able to shear and flatten and the two membranes will nest inside each others folds. The overall thickness of the structure and the spacing between the membranes can be arbitrarily selected by choosing the appropriate rib height.

However, it is not necessary to place ribs on every diagonal crease, or even only on the creases. Depending on the geometry of the structure and the stiffness of the materials used, it may be more appropriate to place ribs at every other crease if the crease spacing is small, or to add additional ribs in between creases if the crease spacing is large. If ribs are placed only at ever other crease, then they will all stack together in the folded structure rather than in two separate groups in the case of ribs at every crease. If additional ribs are necessary, the design would be equivalent to reducing the diagonal crease spacing in the pattern but leaving some of these creases unfolded.

In the case of a two-layer membrane, another alternative arrangement would be to have the membranes folded in an opposite sense, with valley folds on one membrane corresponding to mountain folds on the other, and vice versa.

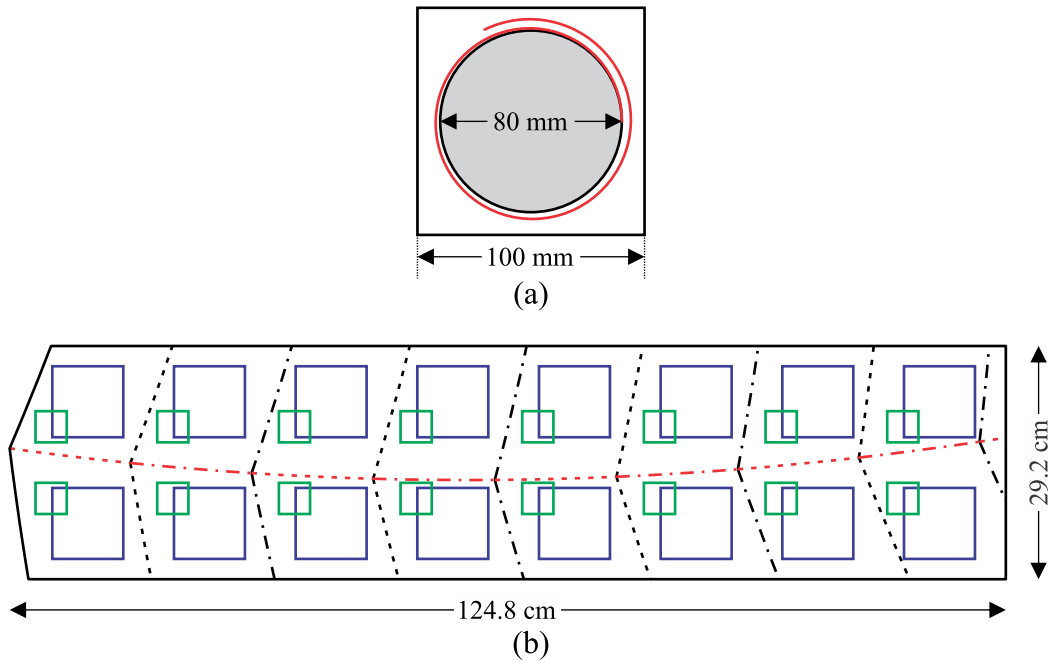


Figure 8. Design for a crease pattern compatible with the antenna array geometry. (a) Packaged configuration showing the centerline crease in red, the round spool (4 cm radius) in gray, and the CubeSat constraints (10 cm square). (b) The crease pattern with antenna components. The centerline crease is shown in red, the radiating patches in blue, and the T/R modules in green. Valley folds are denoted with dashed lines and mountain folds with dash-dotted lines.

This would result in a more symmetrical but taller folded package. This could be beneficial if certain parts of the membrane cannot be folded against each other or if the membrane contains thicker elements that do not stack well in the folded package.

IV. Prototype Fabrication

We used the crease pattern described in the previous section to construct a prototype membrane structure that could support a 2×8 patch antenna array based on the JPL design described in Section II.B. This prototype was constructed using $50 \mu\text{m}$ thick Kapton[®] polyimide film to be consistent with the JPL design. In order to assemble the components of the structure, we chose to use a continuous membrane for one layer, and to cut the other layer into separate panels based on the locations of the ribs. The ribs were attached first to the continuous layer, and then the second layer was attached segment by segment onto the ribs. This is representative of a potential assembly process for the antenna array, since the design includes one continuous layer with the feed network and ground plane, while the other layer only has radiating patches that do not require a physical electrical connection (such as a wire or microstrip trace) to the other membrane or to other locations within the same membrane.

Because of the geometry for this particular design, where the rib length is short relative to the rib spacing, there is a greater tendency for the membrane layers to buckle between the ribs than if the ribs were more closely spaced. To mitigate this effect, thin carbon fiber rods (0.50 mm diameter) were used to stiffen the edges of the membrane. These rods were cut to length based on the crease length of each segment, and were attached along the edges as well as on the longitudinal crease down the center of the structure. Each rod was bonded to the membrane using cyanoacrylate adhesive at the end points and the middle. The rods along the edge of the structure were reinforced with small tabs of polyimide tape to prevent delamination from the membrane. Photos of the prototype fabrication process are included in Figure 9.

The prototype design demonstrated qualitatively good ability to fold and wrap. In total, it was 59 g in mass and covered an area of 0.35 m^2 . This areal density of 0.7 kg/m^2 does not include any supporting structure or the hub, but is very promising in reducing the mass of large planar structures from the current state-of-the-art rigid panel technologies. In order to quantify the deployment behavior of this structure, we conducted deployment experiments with a force sensor, described in the following section.



(a)



(b)



(c)



(d)

Figure 9. Membrane structure fabrication. (a) The bottom membrane layer is a continuous sheet of Kapton® while the top layer is separated into eight panels. (b) Ribs are attached to the bottom layer with short segments of polyimide tape. The top panels are attached in a similar manner to the ribs. (c) Thin carbon rods are attached on the edge of the membrane structure and along the centerline crease in order to stiffen the individual panels. (d) The completed membrane structure.

V. Deployment Experiments

To study the deployment force profile of the membrane structure described in Section IV, the prototype was deployed using a materials testing machine. In order to characterize the forces associated with unwrapping the membrane from a spool, two configurations were tested: the membrane was deployed first from a folded state without being wrapped around a spool, and then from a wrapped and folded state around a rotating hub.

An Instron model 5569 materials testing machine was used to perform the deployment experiments. Because the total length of the membrane structure exceeded the total length of travel of the machine, different configurations were used to study the deployment. The load cell used (model 2525-808) has a range of ± 10 N, with accuracy better than 2.5 mN for indicated loads below 1N, or 0.25% of the indicated load for values greater than 1 N.¹⁸ The load cell can be sampled at an adaptive rate depending on the slope of the previous measurements, up to a maximum of 500 Hz.

The membrane was attached to the load cell using a screw and nut, with a total mass of 4.6 g, connected to a short tab at the tip (midpoint of the deployed end) of the membrane structure. For the unfolding configuration, the root of the membrane structure was fixed to the table surface in front of the machine (28 cm forward and 19 mm below the base of the machine's lowest point of travel). By anchoring the structure below the base of the machine, we were able to capture the end of deployment before reaching the upper limit of travel. However, at the start of the test, the membrane was already deployed to a length of 37 cm. Figure 10 shows the setup for this deployment configuration.

For the unwrapping configuration, a spool was mounted in the machine, centered below the load cell and with the axis of rotation horizontal and 10 cm above the machine's lowest point of travel. The spool is a 5.08 cm (2") diameter aluminum tube with plastic conveyer roller end caps mounted via bushings onto a threaded rod. The mass of the rotating part of the spool is 163.1 g. In order to prevent the membrane structure from unwinding off the spool, it was necessary to impart an external moment on the spool. This was implemented using the counterweight of a 100 g mass on a string, with a pulley used to allow the weight to extend beyond the edge of the table. The string was attached to the surface of the spool and wrapped around it in the opposite direction as the membrane structure. A schematic of the unwrapping configuration is shown in Figure 11 with photos of the setup in Figure 12. Neglecting the transient effect of accelerating the mass up and down as the spool rotates, this configuration provided a constant 25 mNm torque on the spool. Because the spool for the unwrapping configuration is mounted closer to the load cell than the root anchor point in the unfolding configuration, the deployments could start at a deployed length of 10 cm, but could only deploy to a length of 100 cm and not reach the fully deployed length of 125 cm. Deployments were performed at constant speeds ranging from 1 mm/s to 8 mm/s with force measurements sampled at the maximum rate of 500 Hz. During several deployments, video was captured simultaneously. In this paper, results will be discussed from fifteen deployments: eight that were performed from the unfolding configuration, and seven from the unwrapping configuration.

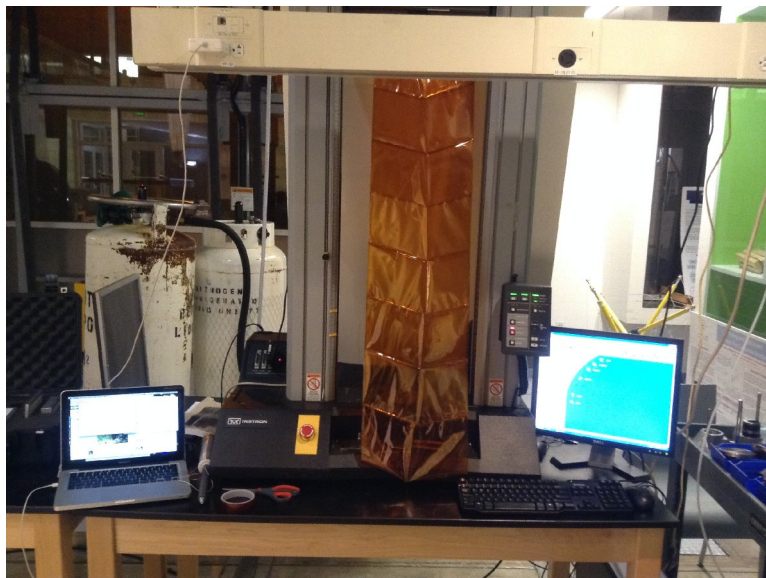


Figure 10. Photo of the membrane structure deployed from the unfolding configuration. The root of the structure was attached to the table in front of the materials testing machine. The tip was attached to the load cell in the machine.

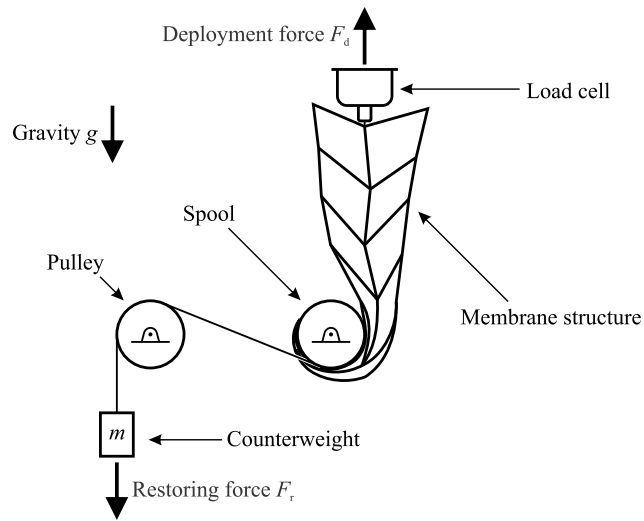
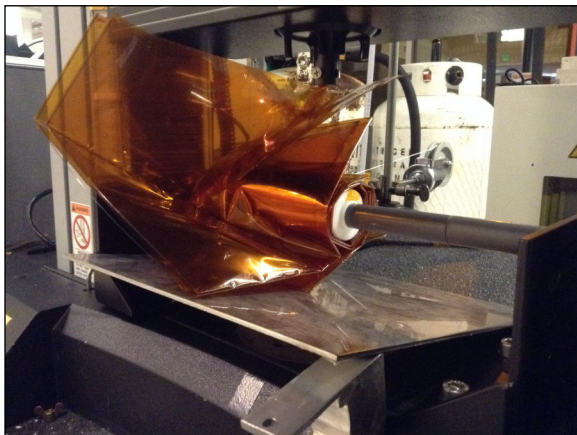
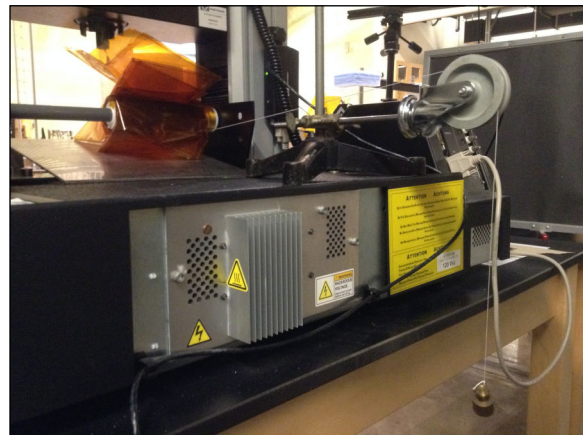


Figure 11. Drawing of the components in the unwrapping configuration. The membrane was attached at the tip to the load cell, and at the root to a spool. The spool was attached to a counterweight through a pulley in order to keep the membrane from unwinding around the spool.



(a)



(b)

Figure 12. Two photos of the experimental setup for the unwrapping configuration, from the (a) front and (b) back of the materials testing machine. The counterweight and pulley can be seen at the back of the machine. An aluminum plate was used to provide a smooth base from which to deploy, so that the membrane would not catch on the fixtures present below the plate.

VI. Experimental Results

With the data collected as described in the previous section, the force profiles for the deployments showed several notable characteristics. The raw measurements are shown in Figure 13. First, the unfolding configuration resulted in a gradual increase in the measured deployment force with a transition to a sharper increase near the end. The gradual increase is attributed primarily to the self weight of the membrane. Second, the unwrapping configuration resulted in a deployment force profile that has several peaks corresponding to the unfolding of the lateral creases in the membrane structure. Finally, during the portions of the unwrapping deployment where the force is generally decreasing, the shape of the force profile is punctuated by a characteristic sawtooth shape with a rapid drop followed by a gradual increase. This can be seen in Figure 14, which shows the deployment force profile for an unwrapping deployment at a rate of 1 mm/s. There is one particular unfolding panel where this does not occur; this anomalous behavior occurred consistently over multiple deployments at a deployment length of 50 to 70 cm, always on the fourth out of seven panels deployed. The data were adjusted to account for disturbances and biases, including the self weight of the membrane and the moment applied to the spool. These were both approximated as linear functions with respect to deployed length. The corrected measurements are shown in Figure 15. Figure 16 shows one unfolding and one unwrapping deployment force profile, along with images of the deployment at 20 cm intervals.

In the following sections, we will look first at the global deployment force profile and how it varies throughout the deployment for the two experimental configurations, and then analyze in more detail the local dynamic behavior that can be seen in some of the measurements.

A. Global deployment force profile

The deployment force profiles appear quite different for the wrapped and unwrapped configurations. When the membrane is only folded but not wrapped around the hub, the deployment force remains quite small and relatively constant. When it is wrapped around the hub, a periodic spike in the deployment force appears, corresponding to the periodicity of the crease pattern. The reason for this increased deployment force compared to the unfolding configuration is that the crease pattern is derived from a Miura-ori design.²⁰ In a conventional Miura-ori fold pattern, the folded membrane behaves as a single degree-of-freedom mechanism: all panels unfold simultaneously. However,

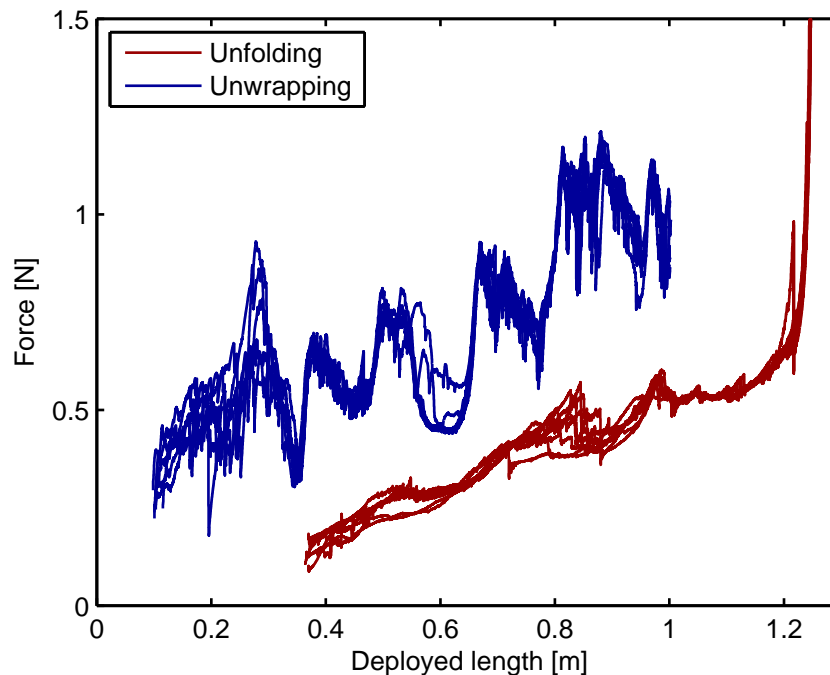


Figure 13. Plot of raw force measurements for all deployments with respect to deployed length. This includes eight unfolding deployments and seven unwrapping deployments.

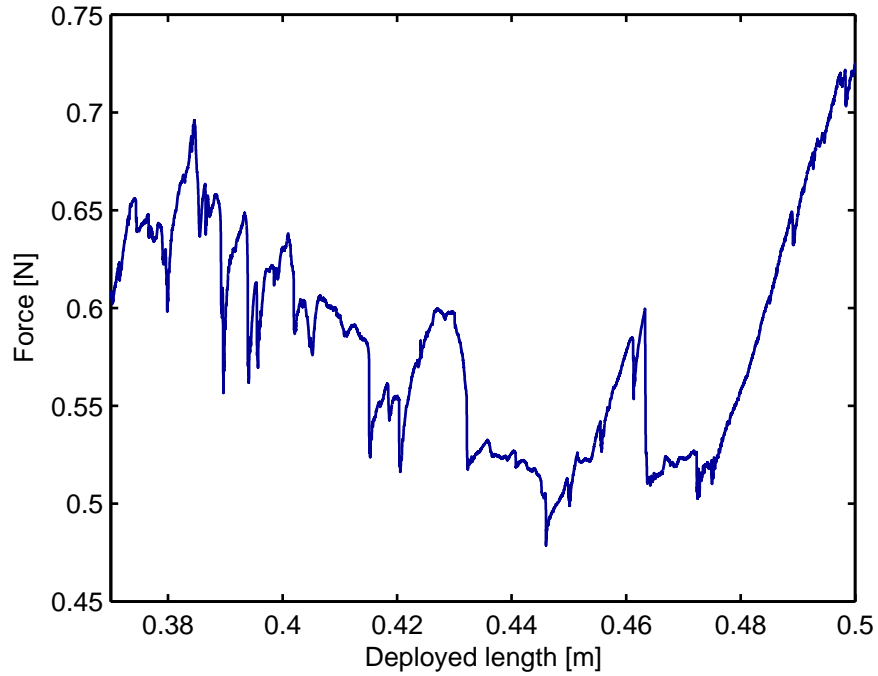


Figure 14. Plot of force measurements for an unwrapping deployment at 1 mm/s. From a deployed length of 37 cm to approximately 47 cm, the deployment force shows a global decrease with characteristic transient features. From 47 cm to 50 cm, the deployment force increases globally and shows fewer of the transients.

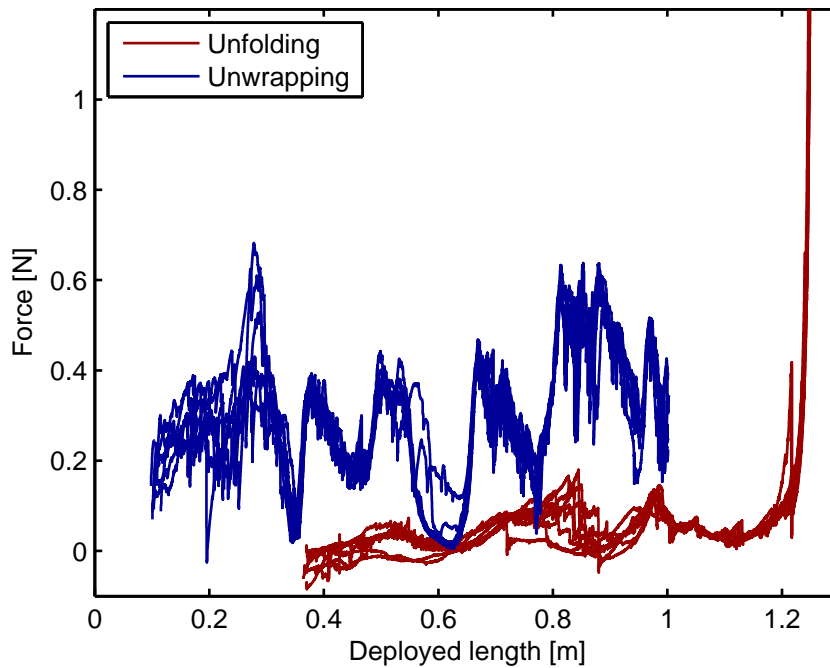


Figure 15. Plot of corrected force measurements for all deployments with respect to deployed length. This includes eight unfolding deployments and seven unwrapping deployments and have been adjusted to remove the effect of self weight of the membrane structure, and for the unwrapping configuration also the effect of the counterweight.

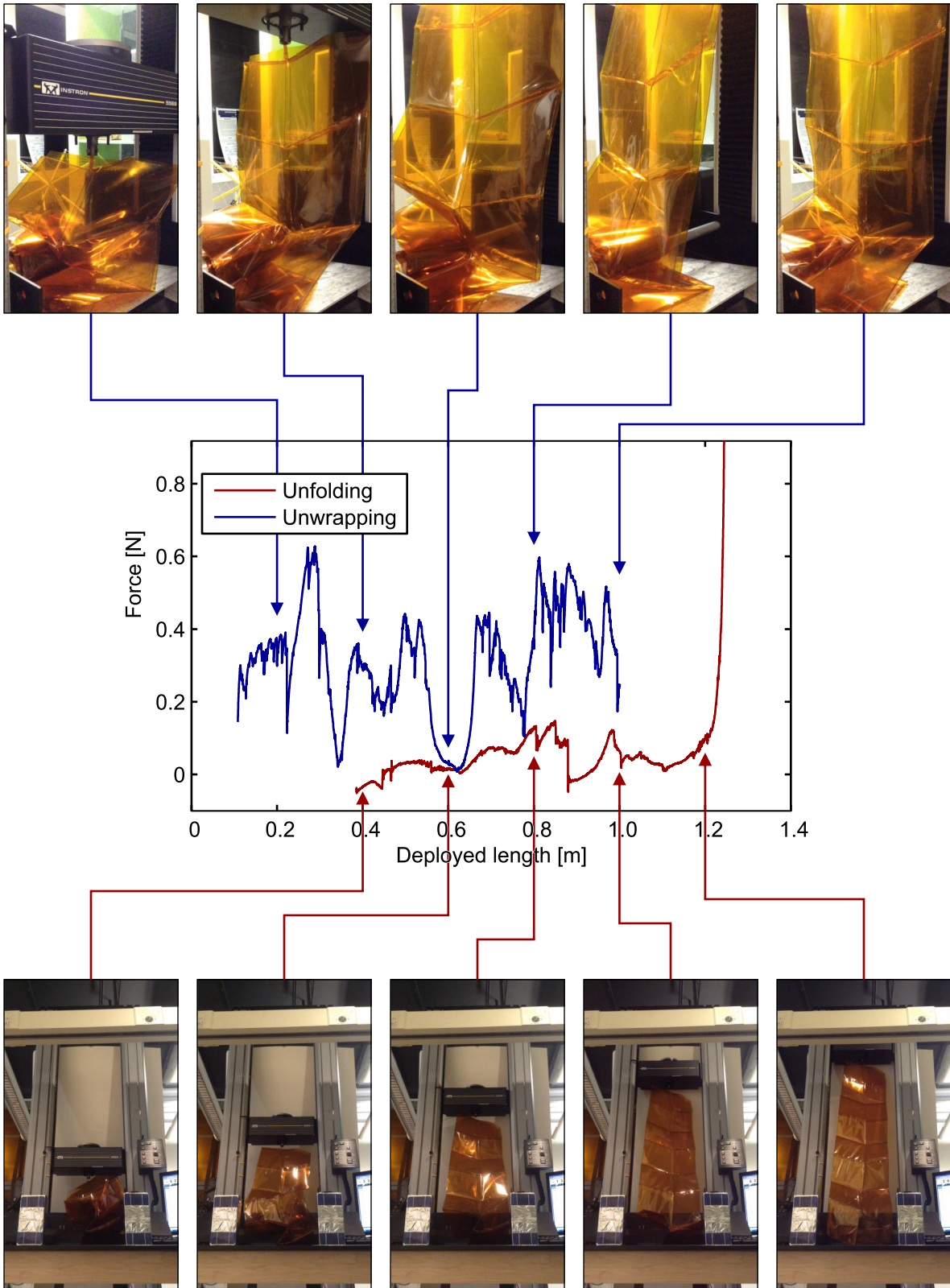


Figure 16. Plot of corrected force measurements for two deployments with respect to deployed length, with photos of the deployed membrane structure. The unfolding deployment, shown in red with the photos below the plot, was performed at 5 mm/s. The unwrapping deployment, shown in blue with the photos above the plot, was performed at 4 mm/s. The photos are shown at equally spaced intervals of 20 cm deployed length for each of the configurations.

in this curved design, the spool prevents the wrapped portion of the structure from unfolding. As a result, each panel must be peeled away from the adjacent panel on the spool, resulting in significant buckling of the membrane surface. As these buckles propagate and the panel lifts off of the spool, the deployment force decreases until the next panel starts to peel away from the spool and the cycle repeats.

The peeling behavior of the wrapped membrane structure results in a deployment force profile that has peaks typically ranging from 0.4 N to 0.8 N, with some spurious peaks up to 1.2 N. This is about an order of magnitude greater than the 0.1 N amplitudes observed in deployment profiles of the unfolding configuration. However, the force required at the end of deployment can greatly exceed the peaks observed in the unwrapping profile, depending on the desired tension or flatness of the membrane. For a practical design, the peaks determine the lower bound of a force profile that would be required to fully deploy the structure. If an actuator did not exert the required force throughout, the deployment would likely be arrested. For a constant force actuator, the deployment force would be determined by the required flatness at the end of deployment, and the fact that the wrapped configuration has a more complex force profile would not be a concern.

From the unfolding configuration, we can see that the deployment force during the final 5% of total deployed length exhibits a sharp increase in slope. This is indicative of the transition from an unfolding mechanism, where hinge moments and membrane buckling provide the dominant resistive force, to a structural process, where the elasticity of the membrane material becomes dominant, and is similar to results obtained for a different crease pattern by Papa and Pellegrino.¹⁹

B. Local dynamic behavior

Within the global behavior of the force profiles for the unwrapping configuration, the regions of decreasing deployment force are predominantly characterized by a sawtooth shape. To study the dynamics of the membrane deployment within this period, we used the spectrogram function in MATLAB[®] to visualize the frequency spectrum of the force profile over time for a series of deployments at rates of 1, 4, and 8 mm/s. These spectrograms use a series of discrete Fourier transforms within a sliding window over the temporal signal. The phase of the spectrogram highlights the characteristic sawtooth transients that occur during the periods of overall decreasing deployment force. Because of the impulsive nature of these features, we expect to see a short period of coherency (constant phase) across a large band in frequency. Spectrograms are plotted for five deployments in Figure 17. Each sawtooth feature corresponds to a transient dynamic event in the membrane deployment. This is attributed to kinks in the membrane that propagate along the surface in short spurts, each time producing a vibration in the structure. For the slowest deployment at 1 mm/s, it appears that many of these features are distinct; the response from one sawtooth is often mostly damped out before the next one occurs. In the faster deployments, there is more overlap between features. This can be seen in a closer view of the spectrogram phase plots in Figure 18. However, the amplitude of the features does not seem to be dependent on deployment rate within the range tested.

In order to better understand the “anomalous” smooth profile associated with the deployment of the fourth panel, the video of the deployment process was analyzed. This panel appears to have unfolded off the spool with significantly less wrinkling than the other panels, as can be seen in Figure 19. This was a result of at least two factors. First, the spool was aligned such that the root of the structure was directly underneath the load cell where the tip was attached. Every other panel was therefore pulled out of the spool at a slightly different angle. The even-numbered panels were unfolded with a force that was better aligned with the direction the panels were moving than the odd-numbered panels. Second, because of the curvature of the centerline crease, each panel width is slightly different on one side of the structure. With the fourth panel, the centerline crease was at its maximum offset from the true centerline of the structure, and there was correspondingly less interaction between that panel and the baseplate.

These findings provide several insights into the requirements for a practical deployment design. Within the range of deployment speeds tested, there does not appear to be any benefit to a slower deployment in reducing the amplitude of the deployment force profile. However, a slower deployment will cause more of the disturbance vibrations from a buckled membrane to damp out before the next impulsive event occurs. For a membrane design that is only characterized to be robust to specific vibration environments, it might be beneficial to avoid the more complex dynamics of interacting vibrations that occur with a faster deployment. Additionally, the housing around a packaged membrane can affect how much wrinkling and buckling will occur in the unfolding panels as the membrane structure deploys. A tight housing will keep the wrapped portion of the membrane closer to the spool and will force each panel to deform more significantly in order to unfold. Ideally, upon deployment, a container holding the membrane would retract completely to avoid adding additional constraints on the deployment process.

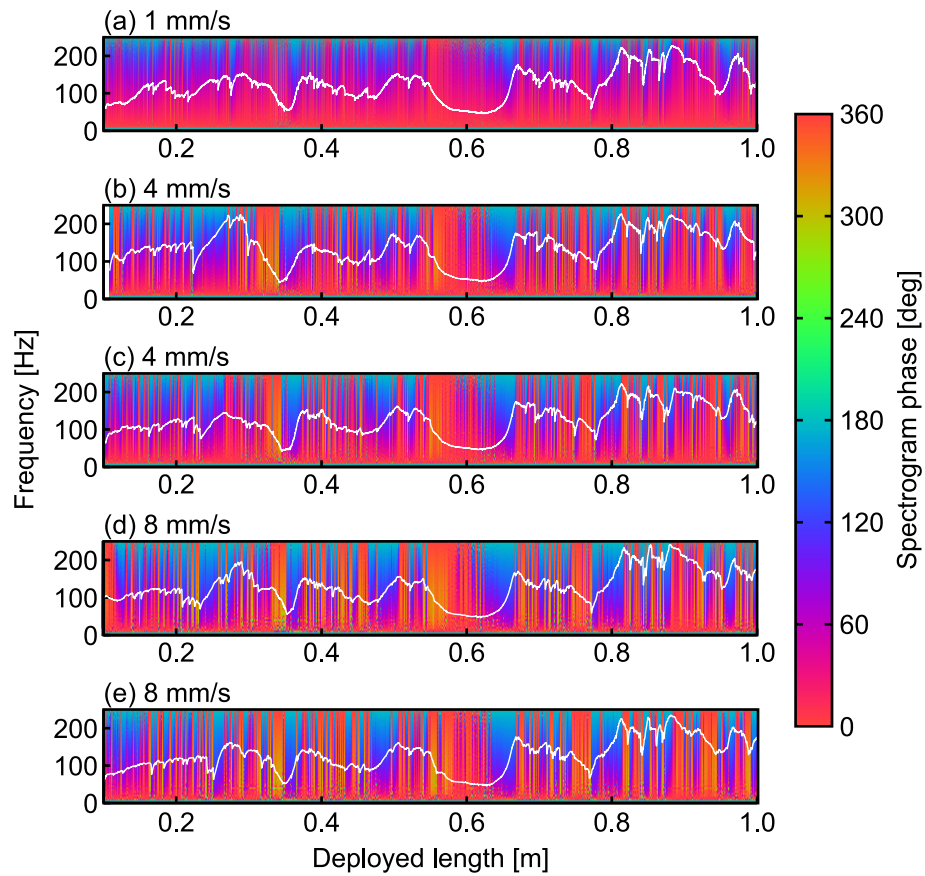


Figure 17. Plot of spectrogram phase for five unwrapping deployments, plotted against deployment length on the horizontal axis. From top to bottom, the deployment rates are (a) 1, (b) 4, (c) 4, (d) 8, and (e) 8 mm/s. The phases are computed from temporal spectrograms with a constant time sliding window of 100 data points, or 0.2 seconds. The slower deployments therefore show a higher spatial resolution over a longer total deployment time. The force measurement is overlaid as the white line on each corresponding spectrogram plot.

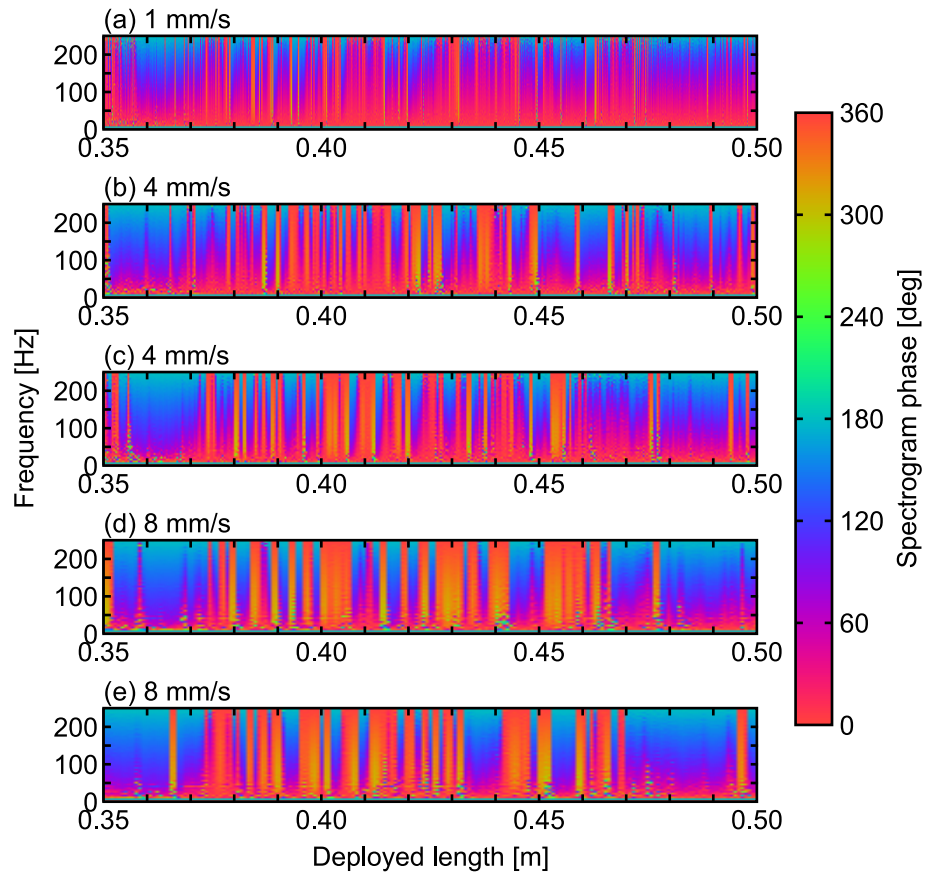


Figure 18. Close up of spectrogram phase for five unwrapping deployments, plotted against deployment length between 0.35 and 0.5 m on the horizontal axis. From top to bottom, the deployment rates are (a) 1, (b) 4, (c) 4, (d) 8, and (e) 8 mm/s. The data are the same as those shown in Figure 17.

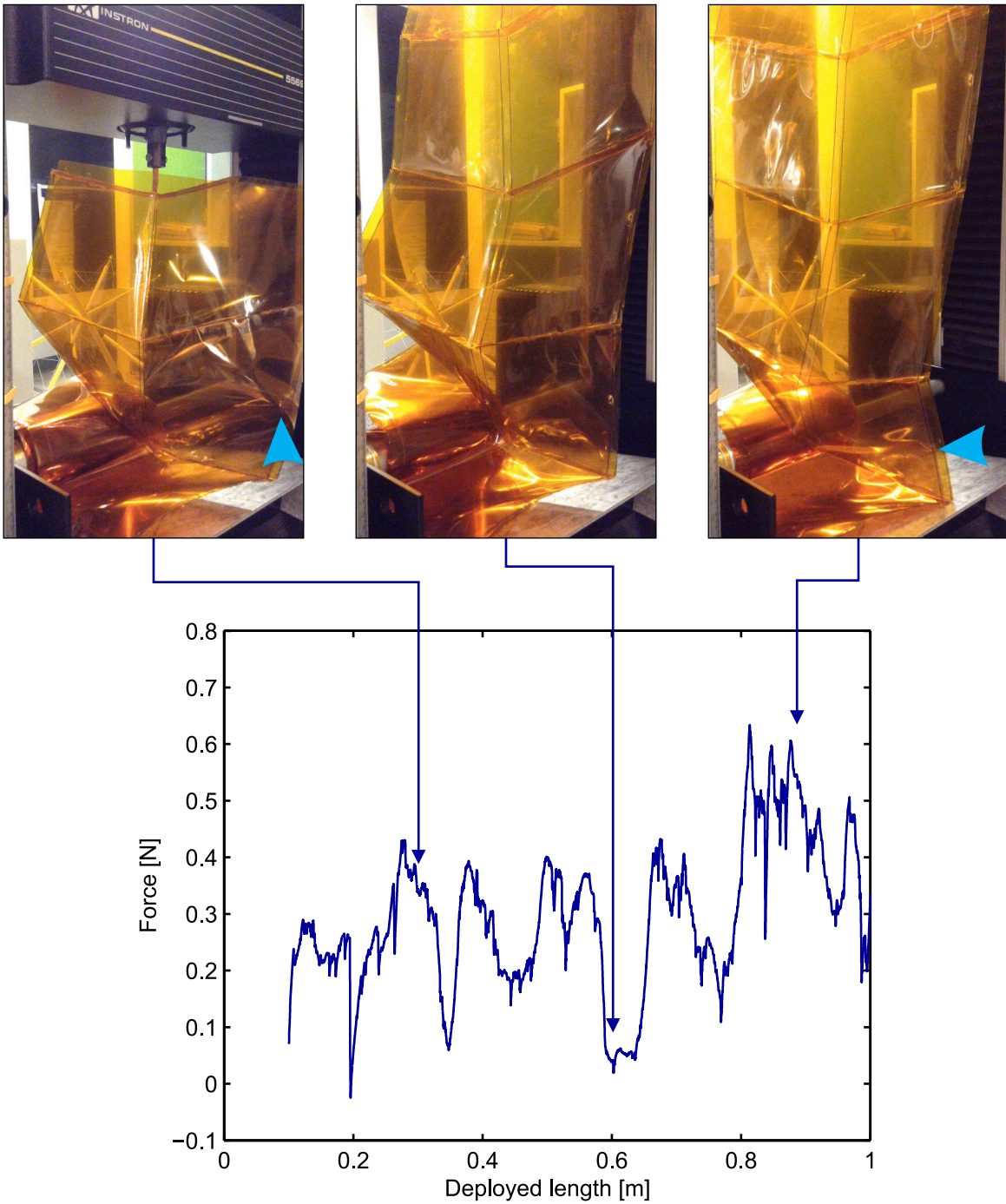


Figure 19. Plot of corrected force measurements for one unwrapping deployment with respect to deployed length, with photos of the deployed membrane structure. The three photos show the second, fourth, and sixth panels unfolding from the spool. In the first and third photos, membrane buckling can be seen, as indicated by the blue arrowheads. The deployment of the fourth panel, without as much buckling, resulted in a lower and smoother force profile.

VII. Conclusions

We have presented a potential membrane structure that is compatible with an existing antenna array design and can be folded and wrapped around a round hub. Through deployment experiments, we measured the deployment force profiles of a prototype membrane structure as it deploys from being wrapped around a spool and as it unfolds without any external constraints. We found that the deployment force required to unwrap the membrane from a spool was an order of magnitude greater than the unfolding force, and that the local dynamic behavior can depend greatly on small deviations in the crease pattern. In the future, we plan to study in more detail the phenomena that occur through the unwrapping process and to better understand the dynamics involved that can affect deployment success.

The membrane structure as designed shows promise in its ability to package panels into a small volume, but further experimentation is required to determine its suitability for deployment with embedded electronics. As a structure supporting an antenna array, the achievable flatness of the membrane surface will need to be characterized.

In addition to the antenna application discussed throughout this paper, this membrane structure design is suitable for other applications, and especially for small spacecraft such as CubeSats, where the size constraints drive many systems to depend on deployable structures. The use of a deployable membrane structure with flexible photovoltaic cells or embedded RF elements has the potential to greatly exceed the size of state-of-the-art hinged solar panels or communications antennas for CubeSats. The geometry of the general folding pattern, with continuous increased sections along the membrane exceeding the dimensions of the packaged volume, can be conducive to embedding electronic components within and on the surface of the structure. The thickness of these components is easily accommodated in the crease design in order to ensure optimal packing efficiency. Additionally, the flexibility in the crease geometry allows each design parameter (rib spacing, crease spacing, and crease angle) to be independently determined by the particular application.

A particular future application of this deployable structure is the capture of small space debris particles between 10 and 100 μm . The growing population of debris is gaining prominence as a significant threat to spacecraft operations, and many different technologies are being proposed to address the problem of active debris removal. The cellular nature of the deployable membrane structure can serve to catch and contain debris particles that a satellite encounters. The two membrane surfaces act as a Whipple shield, fragmenting particles as they penetrate one membrane such that they cannot exit the other side. The fragmented ejecta will therefore remain contained between the membranes and can be further contained by charging the ribs to sweep up the fragments electrostatically. Simultaneously, such a deployed lightweight system on a CubeSat will increase its aerodynamic drag, allowing the spacecraft to launch into higher orbits and maintain compliance with spacecraft lifetime guidelines.

Acknowledgment

N. Lee was supported through this work by a postdoctoral fellowship from the W. M. Keck Institute for Space Studies. We thank P. Arakelian for his assistance with the experimental setup.

References

- ¹Clark, S., "Solar panel shakes loose on Intelsat broadcast satellite," from Spaceflight Now," See <http://http://spaceflightnow.com/sealaunch/is19/120619array/>, 2012.
- ²Miyoshi, K., "Aerospace mechanisms and tribology technology: case study," *Tribology international*, Vol. 32, No. 11, 1999, pp. 673–685.
- ³de Selding, P. B., "SkyTerra 1's Antenna Nearly Fully Deployed," from Space News," See <http://www.spacenews.com/article/skyterra-1s-antenna-nearly-fully-deployed>, 2010.
- ⁴Hoyt, R., Newton, T., Barnes, I., Shepherd, J., Frank, S. S., Slostad, J., Jaroux, B., Twigg, R., et al., "Early Results of the Multi-Application Survivable Tether (MAST) Space Tether Experiment," *21st Annual AIAA/USU Conference on Small Satellites*, 2007.
- ⁵Gilchrist, B. E., Bonifazi, C., Bilén, S. G., Raitt, W. J., Burke, W. J., Stone, N. H., and Lebreton, J. P., "Enhanced electrodynamic tether currents due to electron emission from a neutral gas discharge: Results from the TSS-1R Mission," *Geophysical Research Letters*, Vol. 25, No. 4, 1998, pp. 437–440.
- ⁶Garner, C., Diedrich, B., and Leipold, M., "A Summary of Solar Sail Technology Developments and Proposed Demonstration Missions," *AIAA/ASME/SAE/ASEE, 35th Joint Propulsion Conference and Exhibit*, 1999.
- ⁷Freeland, R. E., Bilyeu, G. D., Veal, G. R., Steiner, M. D., and Carson, D. E., "Large inflatable deployable antenna flight experiment results," *Acta Astronautica*, Vol. 41, No. 4, 1997, pp. 267–277.
- ⁸Guest, S. D. and Pellegrino, S., "Inextensional wrapping of flat membranes," *Structural Morphology: Proc. 1st Int. Sem. Struct. Morphol.*, Montpellier, September 1992, pp. 203–215.
- ⁹Furuya, H., Inoue, Y., and Masuoka, T., "Deployment Characteristics of Rotationally Skew Fold Membrane for Spinning Solar Sail," *46th AIAA/ASME/ASCE/AHS/ASC Structures, Structural Dynamics, & Materials Conference*, AIAA, Austin, TX, 18–21 April 2005.

- ¹⁰Zirbel, S. A., Lang, R. J., Thomson, M. W., Sigel, D. A., Walkemeyer, P. E., Trease, B. P., Magleby, S. P., and Howell, L. L., "Accommodating Thickness in Origami-Based Deployable Arrays," *ASME IDETC*, No. DETC2013-12348, 2013.
- ¹¹Lee, N. and Close, S., "Curved pleat folding for smooth wrapping," *Proceedings of the Royal Society A*, Vol. 469, 2013.
- ¹²Edelstein, W. N., Madsen, S. N., Moussessian, A., and Chen, C., "Concepts and technologies for synthetic aperture radar from MEO and geosynchronous orbits," *Fourth International Asia-Pacific Environmental Remote Sensing Symposium 2004: Remote Sensing of the Atmosphere, Ocean, Environment, and Space*, International Society for Optics and Photonics, 2005, pp. 195–203.
- ¹³Moussessian, A., Del Castillo, L., Bach, V., Grando, M., Quijano, U., Smith, P., and Zawadzki, M., "Large Aperture, Scanning, L-Band SAR," *Earth Science*, 2011.
- ¹⁴Huang, J., Lou, M., Feria, A., and Kim, Y., "An inflatable L-band microstrip SAR array," *Antennas and Propagation Society International Symposium, 1998. IEEE*, Vol. 4, IEEE, 1998, pp. 2100–2103.
- ¹⁵Kobayashi, H., Kresling, B., and Vincent, J. F. V., "The geometry of unfolding tree leaves," *Proceedings of the Royal Society of London. Series B: Biological Sciences*, Vol. 265, No. 1391, 1998, pp. 147.
- ¹⁶Kobayashi, H. and Horikawa, K., "Deployable structures in plants," *Advances in Science and Technology*, Vol. 58, 2008, pp. 31–40.
- ¹⁷Satou, Y. and Furuya, H., "Fold Line Based on Mechanical Properties of Crease in Wrapping Fold Membrane," *54th AIAA/ASME/ASCE/AHS/ASC Structures, Structural Dynamics, and Materials Conference*, AIAA, Boston, MA, 8–1 April 2013.
- ¹⁸Instron, *2525-800 Series Load Cells*, 2005.
- ¹⁹Papa, A. and Pellegrino, S., "Systematically creased thin-film membrane structures," *Journal of Spacecraft and Rockets*, Vol. 45, No. 1, 2008, pp. 10–18.
- ²⁰Miura, K., "Method of packaging and deployment of large membranes in space," *Proc. 31st Congress of the International Astronautical Federation*, Institute of Space and Astronautical Sciences, Tokyo, Japan, September, 1980 1985.